The Astrophysical Journal, 783:100 (11pp), 2014 March 10 doi:10.1088/0004-637X/783/2/100

SIMPLE ANALYTICAL APPROXIMATIONS FOR TREATMENT OF INVERSE COMPTON SCATTERING OF RELATIVISTIC ELECTRONS IN THE BLACKBODY RADIATION FIELD

D. Khangulyan[1], F. A. Aharonian[2,3], and S. R. Kelner[3,4]
[1] Institute of Space and Astronautical Science/JAXA, 3-1-1 Yoshinodai, Chuo-ku, Sagamihara, Kanagawa 252-5210, Japan; khangul@astro.isas.jaxa.jp
[2] Dublin Institute for Advanced Studies, 31 Fitzwilliam Place, Dublin 2, Ireland; Felix.Aharonian@mpi-hd.mpg.de
[3] Max-Planck-Institut für Kernphysik, Saupfercheckweg 1, D-69117 Heidelberg, Germany; Stanislav.Kelner@mpi-hd.mpg.de
[4] National Research Nuclear University, Kashira Highway 31, 115409 Moscow, Russia
Received 2013 October 29; accepted 2014 January 23; published 2014 February 20

ABSTRACT

The inverse Compton (IC) scattering of relativistic electrons is one of the major gamma-ray production mechanisms in different environments. Often, the target photons for IC scattering are dominated by blackbody (or graybody) radiation. In this case, the precise treatment of the characteristics of IC radiation requires numerical integrations over the Planckian distribution. Formally, analytical integrations are also possible but they result in series of several special functions; this limits the efficiency of usage of these expressions. The aim of this work is the derivation of approximate analytical presentations that would provide adequate accuracy for the calculations of the energy spectra of upscattered radiation, the rate of electron energy losses, and the mean energy of emitted photons. Such formulae have been obtained by merging the analytical asymptotic limits. The coefficients in these expressions are calculated via the least-squares fitting of the results of numerical integrations. The simple analytical presentations, obtained for both the isotropic and anisotropic target radiation fields, provide adequate (as good as 1%) accuracy for broad astrophysical applications.

Key words: gamma rays: general – gamma rays: stars – methods: analytical – radiation mechanisms: non-thermal

Online-only material: color figures

1. INTRODUCTION

Relativistic electrons can transfer their energy to gamma rays through the process of inverse Compton (IC) scattering of the ambient low-energy photons. Together with bremsstrahlung, this process represents a major channel to gamma-ray production by relativistic electrons (and positrons). At energies below 100 MeV, a non-negligible contribution to the gamma-ray continuum can be supplied by annihilation of positrons on flight. In the same energy band, one may expect a contribution from the synchrotron radiation of electrons. However, the latter scenario can be effectively realized only in quite unique objects called extreme accelerators, when the particle acceleration proceeds at the maximum (theoretically possible) rate. In general, the synchrotron radiation is released well below the gamma-ray band and, in fact, is considered a dissipative process as long as it concerns the efficiency of gamma-ray production. Indeed, in environments with the energy density of the magnetic field significantly exceeding the energy density of the radiation field, $f = B^2/(8\pi w_{\rm rad}) \gg 1$, only a small fraction (f^{-1}) of the kinetic energy of electrons is released in high-energy gamma rays. Otherwise, the radiative cooling of electrons is dominated by the IC scattering, making the latter an extremely effective gamma-ray production mechanism, especially at very high energies, when the radiative cooling (due to) bremsstrahlung is suppressed compared with the IC scattering.[5] Because of the large cross section of the process and the presence of high-density radiation fields, the IC scattering undoubtedly is the most prolific and universal gamma-radiation mechanism that contributes from low (MeV) to ultrahigh (tens of TeV) energies of emission of almost all nonthermal source populations—supernova remnants (SNR), pulsar wind nebulae (PWNe), compact binary systems, active galactic nuclei (AGNs), etc.

The energy spectrum of the upscattered photons depends strongly on the energy of target photon, especially in the Thomson regime, when the average energy of the upscattered photon is proportional to the energy of the target photon. In the Klein–Nishina regime, the highest fraction of the electron energy is transferred to the upscattered photon, thus the dependence on the target photon energy gradually disappears. Given this non-trivial dependence on the target photon energy, accurate calculations of the IC spectrum require good knowledge of the energy distribution of the target photons. Fortunately, in many cases, the dominant contribution to the IC scattering comes from photons belonging to blackbody (or graybody) radiation, i.e., they are described by the standard Planckian distribution:

$$dN_{\rm ph} \propto \frac{\omega_0^2 d\omega_0}{e^{\omega_0/T} - 1}, \quad (1)$$

where T and ω_0 are the photon gas temperature and the photon energy, respectively (hereafter, the energies of both photons and electrons, as well as the photon gas temperature, are expressed in units of $m_e c^2$).

The Planckian distribution is realized in the case of IC scattering on the 2.7 K cosmic microwave background radiation (CMBR). Remarkably, in SNRs and PWNe in our Galaxy, as well as in extragalactic objects like large-scale AGN jets and clusters of galaxies, the IC scattering in the very high energy band is strongly dominated by CMBR. The target photons for the IC scattering can be well described by the Planckian distribution also in compact systems such as gamma-ray emitting binaries containing either a pulsar (binary pulsars) or a black hole (microquasars). Despite the different origins of the nonthermal

[5] This follows from the ratio of the cooling times due to the bremsstrahlung and IC scattering (in the Thomson regime): $t_{\rm br}/t_{\rm IC} \propto E \times (N_{\rm gas}/w_{\rm rad})$, where E is the electron's energy and $N_{\rm gas}$ is the gas density.

energy, supported in the first case by a rotation-powered pulsar wind and in the second case by an accretion-powered jet, the most likely mechanism of gamma radiation is IC scattering. In both types of objects, the target photons are supplied by the thermal radiation of the bright optical star. Finally, in some cases, quite complex photon distributions can be represented as a superposition of several graybody components.

Since the Planckian distribution of photons is characterized by a rapid decrease in the density both at low and at high energies, numerical integrations of the Compton cross section over the Planckian photon field generally do not impose computational difficulties, but simply require additional computational time. Often, to shorten the calculations, different approximations are used. The most common approach is the δ-functional approximation for the narrow Planckian spectrum. This approximation can correctly describe the lower energy part of the spectrum, but is not applicable for the precise computations of the entire gamma-ray spectra (see Section 6). Therefore, some other approximations for calculations of IC spectra have been recently suggested in the literature (see Petruk 2009; Zdziarski & Pjanka 2013). These approaches provide a better description for the IC spectra and are characterized by a higher precision than the δ-functional approximation is, although they are not free of certain limitations (see the discussion in Section 6).

In this paper, we propose new, very simple analytical presentations obtained for both isotropic and mono-directional angular distributions of a target radiation field assuming that its energy spectrum is precisely described by the Planckian distribution. We provide analytical formulae for the energy spectra of upscattered radiation, as well as for the interaction and the energy-loss rates of electrons. The "threshold" for the accuracy of these formulae in all cases has been set at a level of 1%.

2. APPROXIMATE DESCRIPTION OF THE IC PROCESS

The interaction of electrons with photons is described with the standard means of quantum electrodynamics. In the astrophysical context, the general expressions for the Compton cross section can be significantly simplified using the fact that the energy of the target photons is typically small, $\omega_0 \ll 1$, and that the electrons are relativistic, $E \gg 1$ (this condition, in particular, implies that the upscattered photon moves in the direction of the initial velocity of the electron). Under these circumstances, for the target photons with a fixed direction, the scattering rate by an electron moving with a velocity that makes an angle θ with the photon's direction has the following simple form (Aharonian & Atoyan 1981):

$$\frac{d\nu_{\rm ani}}{d\omega\, dN_{\rm ph}\, dt} = c(1-\cos\theta)\frac{d\sigma}{d\omega} = \frac{4\pi c r_0^2 (1-\cos\theta)}{b_\theta E} \times \left[1 + \frac{z^2}{2(1-z)} - \frac{2z}{b_\theta(1-z)} + \frac{2z^2}{b_\theta^2(1-z)^2}\right], \quad (2)$$

where E, $\omega_0 = b_\theta/[2E(1-\cos\theta)]$, and $\omega = zE$ are the energies of the electron, soft photon, and upscattered photon, respectively, $r_0 = e^2/(m_{\rm e}c^2)$ is the electron classical radius, and $N_{\rm ph}$ is the number of target photons per unit of volume. If the target photon field is isotropic, the above expression should be averaged over the interaction angle (Aharonian & Atoyan 1981):

$$\frac{d\nu_{\rm iso}}{d\omega\, dN_{\rm ph}\, dt} = c\int(1-\cos\theta)\frac{d\sigma}{d\omega}\frac{d\Omega}{4\pi} = \frac{8\pi c r_0^2}{bE}\left[1 + \frac{z^2}{2(1-z)} + \frac{z}{b(1-z)} - \frac{2z^2}{b^2(1-z)^2} - \frac{z^3}{2b(1-z)^2} - \frac{2z}{b(1-z)}\log\frac{b(1-z)}{z}\right], \quad (3)$$

where $b = 4\omega_0 E$ is the Klein–Nishina parameter and the notation log is used for logarithm to the base e, i.e., the "natural logarithm." Note that Equation (3) has been originally derived by Jones (1968) in a straightforward way, without using the intermediate angle-dependent rate given by Equation (2) (for a review, see Blumenthal & Gould 1970).

In the case of blackbody target photons, the scattering rates given by Equations (2) and (3) should be integrated over the Planckian distribution of target photons:

$$dN_{\rm ph} = \frac{m_{\rm e}^3 c^3 \kappa}{\pi^2\hbar^3}\frac{\omega_0^2\, d\omega_0}{{\rm e}^{\omega_0/T}-1}, \quad (4)$$

where κ is the dilution factor in the case of graybody radiation. The lower integration limit, $\omega_0 \geqslant \epsilon_{\rm ani/iso}$, is determined by the kinematic conditions (i.e., conditions imposed by the conservation of 4-momentum) as

$$\epsilon_{\rm ani} = \frac{\omega}{2E}\frac{1}{(E-\omega)}\frac{1}{(1-\cos\theta)} = \frac{z}{1-z}\frac{T}{t_\theta} \quad (5)$$

and

$$\epsilon_{\rm iso} = \frac{\omega}{4E}\frac{1}{(E-\omega)} = \frac{z}{1-z}\frac{T}{t} \quad (6)$$

for the cases of mono-directional and isotropic photon distributions, respectively. Here, the following notations are used: $t_\theta = 2ET(1-\cos\theta)$ and $t = 4ET$.

Formally, for large values of $\omega_0 \to +\infty$, Equations (2) and (3) are not applicable, since the basic assumption, $\omega_0 \ll \omega$, used for the derivation of these expressions fails. However, assuming a non-relativistic photon temperature $T \ll 1$, one can safely extend the integration upper limit to $+\infty$. Therefore, the interaction rate with a blackbody distribution of target photons is

$$\frac{dN_{\rm ani/iso}}{d\omega\, dt} = \frac{T^3 m_{\rm e}^3 c^3 \kappa}{\pi^2\hbar^3}\int_{\epsilon_{\rm ani/iso}/T}^{\infty}\frac{d\nu_{\rm ani/iso}}{d\omega\, dN_{\rm ph}\, dt}\frac{x^2 dx}{{\rm e}^x - 1}. \quad (7)$$

The substitution of Equations (2) and (3) into Equation (7) leads to an expression that can be presented in a form that contains the following functions introduced by Zdziarski & Pjanka (2013) (Equations (15) and (29) in their paper):

$$f_i = \int_{x_0}^{\infty}\frac{x^i\, dx}{{\rm e}^x - 1}, \quad (8)$$

for $i = -1$, 0, and +1 and

$$f_{\rm ln} = \int_{x_0}^{\infty}\frac{\log(x)\, dx}{{\rm e}^x - 1}, \quad (9)$$

while the integral f_0 is expressed through elementary functions:

$$f_0 = -\log(1-{\rm e}^{-x_0}) \quad (10)$$

and f_{+1} allow for a representation with a dilogarithm function (see Equation (7) of Zdziarski & Pjanka 2013). The two other functions (f_{-1} and $f_{\ln}$), as shown by Zdziarski & Pjanka (2013), can be expressed through series (Equations (14) and (28) of Zdziarski & Pjanka 2013). However, each of these terms contains special functions, which makes the usage of these expressions rather inconvenient.

We use a different approach to obtain approximate formulae for the IC cross section. First, we present the cross section in a form containing strictly positive terms. This dramatically reduces the risk of large mistakes because of the summation of rounding errors. Furthermore, we approximate these terms by simple analytical expressions. The derivations of these expressions are based on analytical computations of the asymptotic limits and the introduction of correction functions for the intermediate range of energies by invoking a least-squares fit. This allows us to present Equation (7) in a form that contains only elementary functions.

For the case of a mono-directional photon field, Equation (7) can be expressed as

$$\frac{dN_{\rm ani}}{d\omega\, dt} = \frac{2r_o^2 m_{\rm e}^3 c^4 \kappa T^2}{\pi\hbar^3 E^2}\left[\frac{z^2}{2(1-z)}F_1(x_0) + F_2(x_0)\right], \quad (11)$$

where $x_0 = (z/(1-z)t_\theta)$ and the positive functions F_1 and F_2 are determined as

$$F_1(x_0) = f_{+1}(x_0), \quad (12)$$

$$F_2(x_0) = f_{+1}(x_0) + 2x_0^2 f_{-1}(x_0) - 2x_0 f_0(x_0)\,. \quad (13)$$

For the case of an isotropic photon field, Equation (7) takes the following form:

$$\frac{dN_{\rm iso}}{d\omega\, dt} = \frac{2r_o^2 m_{\rm e}^3 c^4 \kappa T^2}{\pi\hbar^3 E^2}\left[\frac{z^2}{2(1-z)}F_3(x_0) + F_4(x_0)\right], \quad (14)$$

where $x_0 = z/(1-z)t$. The positive functions F_3 and F_4 are expressed via f_{-1}, f_0, f_{+1}, and $f_{\ln}$:

$$F_3(x_0) = f_{+1}(x_0) - x_0 f_0(x_0) \quad (15)$$

and

$$\begin{aligned} F_4(x_0) = {} & (f_{+1}(x_0) - x_0 f_0(x_0)) \\ & + 2x_0(\log(x_0) f_0(x_0) - f_{\ln}(x_0)) \\ & + 2x_0(f_0(x_0) - x_0 f_{-1}(x_0)). \end{aligned} \quad (16)$$

Thus, the IC radiation spectra can be presented in simple analytical forms of Equations (11) and (14) as functions of the variable z through the term $z^2/(2(1-z))$ and the four functions F_1, F_2, F_3, and F_4. All of these functions depend only on the parameter x_0, which is equal to $z/((1-z)t_\theta)$ and $z/((1-z)t)$ in the case of mono-directional and isotropic photon fields, respectively.

The functions F_1 and F_2 have the same asymptotic limits:

$$F_{1,2} = \begin{cases} \frac{\pi^2}{6}, & x_0 \ll 1 \\ x_0 {\rm e}^{-x_0}, & x_0 \gg 1 \end{cases}. \quad (17)$$

A simple function with the similar asymptotic behavior can be used as a zeroth-order approximation for the functions F_1 and F_2 (see Figure 1):

$$G_{1,2}^{(0)} = \left(\frac{\pi^2}{6} + x_0\right){\rm e}^{-x_0}\,. \quad (18)$$

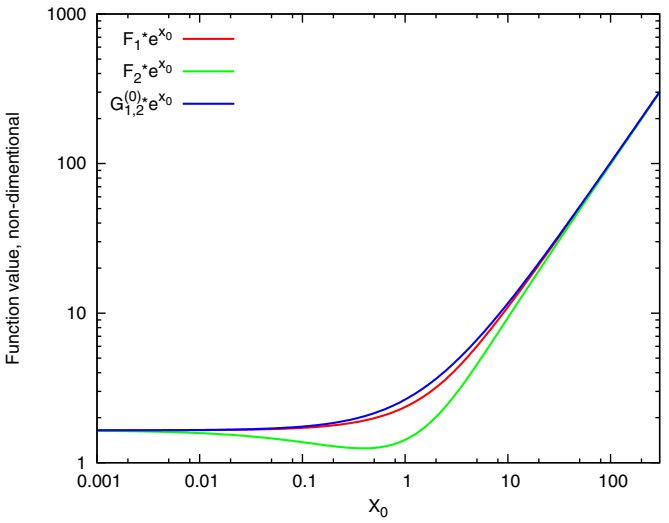

Figure 1. Functions F_1 and F_2 are shown together with the zeroth-order approximation $G_1^{(0)}$ (the function $G_2^{(0)}$ is equal to $G_1^{(0)}$). The function $G_1^{(0)}$ reproduces the asymptotic behavior of functions $F_{1,2}$, but differs by a factor $\lesssim 2$ for $x_0 \sim 1$.

(A color version of this figure is available in the online journal.)

A numerical comparison of these functions shows that $G_1^{(0)}$ provides[6] an accuracy of 10% and 50% for F_1 and F_2, respectively. To improve the accuracy, we introduce correction functions:

$$G_{1,2} = G_{1,2}^{(0)}(x_0) \times g_{1,2}(x_0), \quad (19)$$

We present the correction factors g_1 and g_2 as functions of the variable x_0 with four free parameters:

$$g_i(x_0) = \left[1 + \frac{a_i x_0^{\alpha_i}}{1 + b_i x_0^{\beta_i}}\right]^{-1}. \quad (20)$$

The parameters $\alpha_i > 0, a_i, \beta_i > \alpha_i, b_i > 0$ were used for the least-squares fitting of the functions $F_{1,2}$. Obviously, this is not a unique representation for the approximation function, but since $g \to 1$ for $x \ll 1$ and $x \gg 1$, the considered function family should preserve the asymptotic behavior of the zeroth-order fit $G_{1,2}^{(0)}$ and provide enough freedom for fitting. We therefore use Equation (20) as the correction function for fitting procedures used in this paper.

The numerical least-squares fitting gives the following sets of parameters:

$$\begin{aligned} \alpha_1 &= 0.857, \quad a_1 = 0.153, \\ \beta_1 &= 1.84, \quad b_1 = 0.254 \end{aligned} \quad (21)$$

and

$$\begin{aligned} \alpha_2 &= 0.691, \quad a_2 = 1.33, \\ \beta_2 &= 1.668, \quad b_2 = 0.534, \end{aligned} \quad (22)$$

which provide a precision of better than 1% for the entire range of x_0, as shown in Figures 2 and 3.

[6] The functions $G_1^{(0)}$ and $G_2^{(0)}$ are identical.

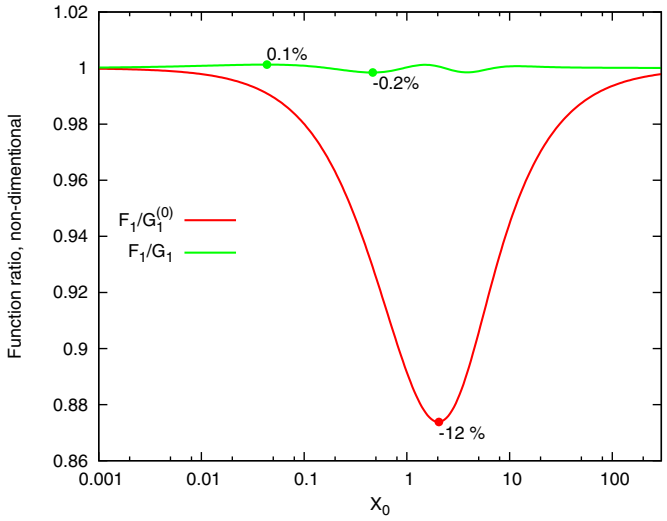

Figure 2. Ratios of the function F_1 to the approximations $G_1^{(0)}$ and G_1.
(A color version of this figure is available in the online journal.)

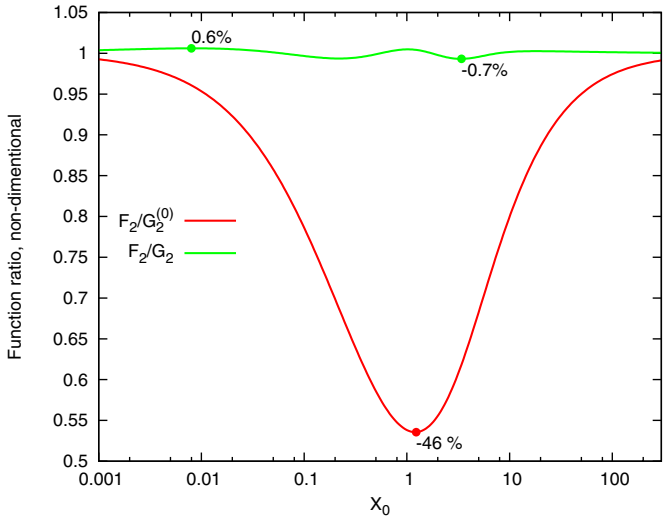

Figure 3. Ratios of the function F_2 to the approximations $G_2^{(0)}$ and G_2.
(A color version of this figure is available in the online journal.)

A similar approach can be used for the approximation of the angle-averaged IC spectra determined by Equation (14). The functions F_3 and F_4 have the same asymptotic:

$$F_{3,4} = \begin{cases} \frac{\pi^2}{6}, & x_0 \ll 1 \\ \mathrm{e}^{-x_0}, & x_0 \gg 1 \end{cases}, \tag{23}$$

which suggests the following family of approximation functions:

$$G_{3,4} = G_{3,4}^{(0)}(x_0) \times g_{3,4}(x_0), \tag{24}$$

where

$$G_{3,4}^{(0)}(x_0) = \frac{\pi^2}{6} \frac{1 + c_{3,4}\, x_0}{1 + \frac{\pi^2 c_{3,4}}{6} x_0} \mathrm{e}^{-x_0}. \tag{25}$$

The functions $G_{3,4}^{(0)}$ have a similar asymptotic behavior as the functions $F_{3,4}$, as demonstrated in Figure 4. Here, $c_{3,4} > 0$ are parameters that do not change the asymptotic behavior of $G_{3,4}^{(0)}$. Therefore, they can be optimized for a better description of the functions $F_{3,4}$. In particular, for the value of $c_3 = 2.73$, the

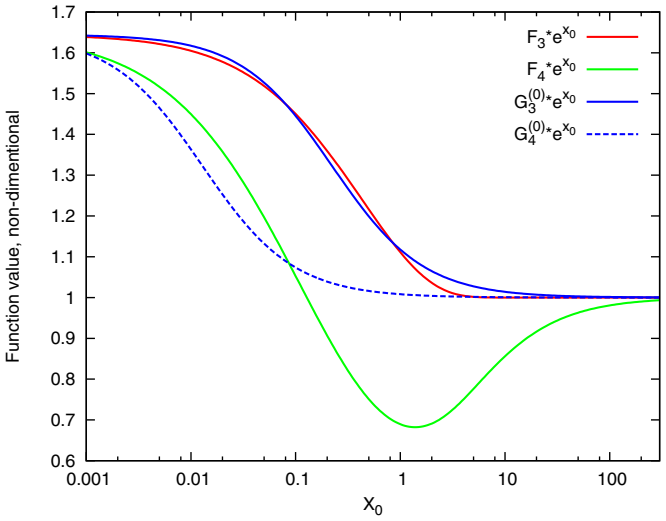

Figure 4. Functions F_3 and F_4 are shown together with the zeroth-order approximations $G_3^{(0)}$, computed for $c_3 = 2.73$, and $G_4^{(0)}$, computed for $c_4 = 47.1$.
(A color version of this figure is available in the online journal.)

function $G_3^{(0)}$ provides a 3% accuracy for the function F_3, as shown in Figure 4.

As can be seen in Figure 4, the function $F_4 \times \mathrm{e}^{x_0}$ features a ∼30% dip at $x_0 \sim 1$, which cannot be reproduced by the function $G_4^{(0)}$. Therefore, the parameter c_4 alone cannot provide an approximation with precision better than a 30% for the function F_4 (such accuracy can be achieved for $c_4 \simeq 50$). However, Equation (24) provides a five-parameter ($a_{3,4}$, $\alpha_{3,4}$, $b_{3,4}$, $\beta_{3,4}$, and $c_{3,4}$) function family that can be used for fitting functions $F_{3,4}$. The numerical least-squares fits resulted in the following sets of parameters:

$$\begin{aligned} \alpha_3 &= 0.606, \quad a_3 = 0.443, \\ \beta_3 &= 1.481, \quad b_3 = 0.54, \\ & \quad\; c_3 = 0.319, \end{aligned} \tag{26}$$

and

$$\begin{aligned} \alpha_4 &= 0.461, \quad a_4 = 0.726, \\ \beta_4 &= 1.457, \quad b_4 = 0.382, \\ & \quad\; c_4 = 6.62, \end{aligned} \tag{27}$$

which gave a <1% precision for the entire range of x_0, as shown in Figures 5 and 6.

The parameterizations for the functions F_1, F_2, F_3, and F_4 given by Equations (19) and (24), with corresponding parameters from Equations (21)–(22) and (26)–(27), allow us to describe the IC spectra, Equations (11) and (14), with a precision better than 1%. Note that this value corresponds to the maximum deviation of the approximate formulae from the precise value; in the case of a broad distribution of electrons, the accuracies obviously will be significantly better.

The approximations obtained above describe the IC spectra for two different, isotropic, and mono-directional angular distributions of target photons. The former scenario with an involvement of the CMBR is often realized in different objects like SNRs, PWNe, and clusters of galaxies. However, in many other cases, the background photon field can be approximated as a graybody (or a superposition of a several graybody components). In this case, the energy, ω_*, at which the spectral energy distribution (i.e., νF_ν) of target photons achieves the maximum

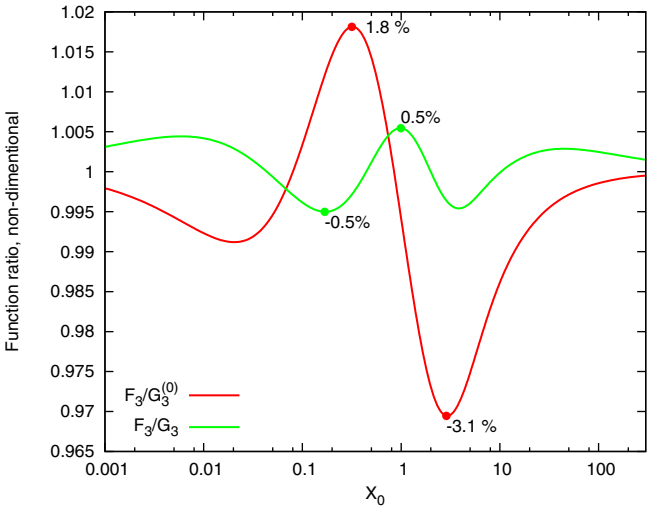

Figure 5. Ratios of the function F_3 to the approximations $G_3^{(0)}$ (taken for $c_3 = 2.73$) and G_3. The fitting parameters used are indicated by Equation (26). (A color version of this figure is available in the online journal.)

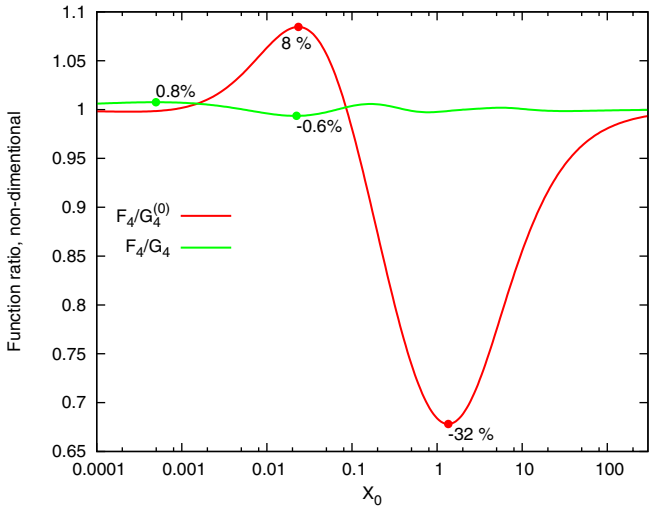

Figure 6. Ratios of the function F_4 to the approximations $G_4^{(0)}$ (taken for $c_4 = 47.1$) and G_4. We show this plot for an increased range of x_0, as compared with Figures 1–5, to include the region where the ratio of F_4 to G_4 achieves its maximum.

(A color version of this figure is available in the online journal.)

allows us to define the temperature of the graybody emission:

$$T = 0.255\,\omega_* . \tag{28}$$

The energy density of the target photon field, w_*, allows us then to obtain the corresponding dilution coefficient:

$$\kappa = 360\frac{\hbar^3 w_*}{m_e^3 c^5}\left(\frac{\omega_*}{m_e c^2}\right)^{-4} . \tag{29}$$

The approximation of a mono-directional photon field is applicable when the source of the target photons is compact; namely, in the IC production region, the value of $(1-\cos\theta)$ should not vary significantly for the photons coming from different regions of the source. Then, in the IC production site, the target photon field is typically diluted by a factor

$$\kappa = \frac{\Delta\Omega}{4\pi}, \tag{30}$$

where $\Delta\Omega \ll 1$ is the solid angle of the target photons' source, as seen from the IC production region. In case the source of the target photons is a star, Equation (30) can be expressed through the radius, R_*, of the star and the distance, R, between the IC emitter and the star (the condition $\Delta\Omega \ll 1$ is realized if $R \gg R_*$):

$$\kappa = \left(\frac{R_*}{2R}\right)^2 . \tag{31}$$

3. THE RATE OF IC LOSSES

IC energy losses of a particle in a Planckian photon field can be expressed as

$$\dot{E}_{\rm ani/iso} = \frac{m_e^3 c^3 \kappa E^2}{\pi^2\hbar^3}\int_0^\infty d\omega_0 \frac{\omega_0^2}{e^{\omega_0/T}-1}\int_0^{z_{\rm max}} dz z \frac{d\nu_{\rm ani/iso}}{d\omega dN_{\rm ph}\,dt}, \tag{32}$$

where $z_{\rm max}$ is $b/(1+b)$ or $b_\theta/(1+b_\theta)$ for isotropic and mono-directional photon fields, respectively. Formally, the integration lower limit is not equal to 0, however, the contribution to the integral from the region of small z is negligible. Therefore, we formally set the lower limit to 0.

The structure of Equation (32) allows us to determine the dependence of the energy-loss rate on the electron energy and photon field temperature. Namely, if the IC scattering proceeds with a fixed interaction angle, one obtains

$$\begin{aligned}\dot{E}_{\rm ani} &= \frac{r_0^2 m_e^3 c^4 \kappa}{2\pi\hbar^3 (E(1-\cos\theta))^2}\int_0^\infty db_\theta \frac{b_\theta}{e^{b_\theta/t_\theta}-1} \\ &\times \int_0^{\frac{b_\theta}{(1+b_\theta)}} dz\, z\left[1+\frac{z^2}{2(1-z)}-\frac{2z}{b_\theta(1-z)}+\frac{2z^2}{b_\theta^2(1-z)^2}\right] \\ &= \frac{2r_0^2 m_e^3 c^4 \kappa T^2}{\pi\hbar^3} F_{\rm ani}(t_\theta).\end{aligned} \tag{33}$$

Based on the asymptotic behavior of the function $F_{\rm ani}$:

$$F_{\rm ani}(u) = \begin{cases} \frac{\pi^4}{45}u^2 = 2.16u^2, & u \ll 1 \\ \frac{\pi^2}{12}\,\log(u) = 0.822\log(u), & u \gg 1, \end{cases} \tag{34}$$

we suggest the following approximate presentation for the function $F_{\rm ani}$:

$$G_{\rm ani}^{(0)}(u) = \frac{c_{\rm ani}\, u\log(1+2.16u/c_{\rm ani})}{1+c_{\rm ani}\,u/0.822} . \tag{35}$$

Least-squares fitting for the parameter $c_{\rm ani}$ results in $c_{\rm ani} = 6.13$, for which Equation (35) provides an accuracy of an order of 1% (see Figure 7).

Similarly, if IC cooling proceeds with isotropized scattering angles, the energy loss rate is

$$\begin{aligned}\dot{E}_{\rm iso} &= \frac{r_0^2 m_e^3 c^4 \kappa}{8\pi\hbar^3 E^2}\int_0^\infty db \frac{b}{e^{b/t}-1}\int_0^{\frac{b}{(1+b)}} dz\, z \\ &\times\left[1+\frac{z^2}{2(1-z)}+\frac{z}{b(1-z)}-\frac{2z^2}{b^2(1-z)^2}-\frac{z^3}{2b(1-z)^2}\right. \\ &\left.-\frac{2z}{b(1-z)}\log\frac{b(1-z)}{z}\right] = \frac{2r_0^2 m_e^3 c^4 \kappa T^2}{\pi\hbar^3} F_{\rm iso}(t).\end{aligned} \tag{36}$$

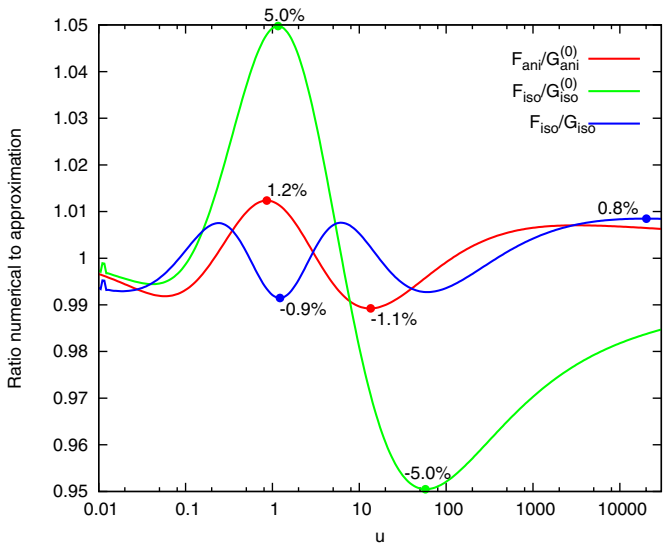

Figure 7. Ratio of the function $F_{\rm ani}$ to $G^{(0)}_{\rm ani}$ (for $c_{\rm ani} = 6.13$) and $F_{\rm iso}$ to $G^{(0)}_{\rm iso}$ (for $c_{\rm iso} = 4.62$) and $G^{(0)}_{\rm iso} \times g(u)$.

(A color version of this figure is available in the online journal.)

The asymptotic behavior of function $F_{\rm iso}$ is similar to Equation (34):

$$F_{\rm iso}(u) = \begin{cases} \frac{\pi^4}{135} u^2 = 0.722 u^2, & u \ll 1 \\ \frac{\pi^2}{12}\ \log(u) = 0.822\ \log(u), & u \gg 1. \end{cases}, \quad (37)$$

Therefore, we can use a function similar to Equation (35):

$$G^{(0)}_{\rm iso}(u) = \frac{c_{\rm iso} u \log(1 + 0.722 u/c_{\rm iso})}{1 + c_{\rm iso} u/0.822}. \quad (38)$$

Least-squares fitting for this function renders a value of $c_{\rm iso} = 4.62$, for which Equation (38) provides a ~5% precision (see Figure 7). This approximation can be improved by using the correction function defined by Equation (20). In particular, a set of the parameters

$$\begin{array}{ll} \alpha_{\rm iso} = 0.682, & a_{\rm iso} = -0.362, \\ \beta_{\rm iso} = 1.281, & b_{\rm iso} = 0.826, \\ & c_{\rm iso} = 5.68 \end{array} \quad (39)$$

provides a ~1% precision (see Figure 7). A similar expression (although less optimized, with an accuracy of 3%) was originally presented in Bosch-Ramon & Khangulyan (2009).

The equation obtained for $F_{\rm ani}$ (Equation (35)) and Equations (38)–(39) for $F_{\rm iso}$ allow a precise description of the energy losses with formulae Equations (33) and (36), which correspond to the case of electron–photon interactions at a specific angle and angle-averaged, respectively. It is important to note that the latter can be realized also in cases when the target photons are mono-directional in the source frame. For example, if particles are isotropized by the source magnetic field, the production of the IC emission toward the observer proceeds at a specific interaction angle, since relativistic particles emit within a narrow cone in the direction of their motion. However, if the IC cooling time exceeds the particle isotropization timescale, each particle can interact with photons at an arbitrary angle and therefore particle losses are effectively determined by the interaction with an isotropic photon field, i.e., by Equation (36).

The particle cooling described by Equation (33) can be realized, for example, in the so-called Compton-drag scenarios, i.e., when the temperature of the emitting particles is very small and the bulk motion component is dominant. In particular, this may be relevant to the pulsar-wind zone for pulsars located in systems with bright stars (see, e.g., Khangulyan et al. 2007, 2011). Also, a similar situation can arise if the IC cooling time is shorter than the isotropization timescale.

Often, it is convenient to characterize the energy losses through the cooling time:

$$t_{\rm ic} = \frac{E}{\dot{E}} = \frac{\pi \hbar^3}{2 r_0^2 m_{\rm e}^3 c^4 \kappa T^2} \frac{E}{F_{\rm ani/iso}\left(t_{\theta/.}\right)}. \quad (40)$$

In the Thomson limit, for the case of an isotropic photon field, this expression gives

$$t_{\rm ic} = \left(\frac{4cE}{3} \frac{\pi^2 \kappa T^4 m_{\rm e}^3 c^3}{15 \hbar^3} \frac{8\pi r_0^2}{3} \right)^{-1}, \quad (41)$$

where the middle term corresponds to the ratio of energy density of the blackbody photon distribution to $m_{\rm e}c^2$.

It was suggested in Aharonian et al. (2006) and further generalized by Bosch-Ramon & Khangulyan (2009) that, in the case of an isotropic photon field, the IC cooling time in the Klein–Nishina limit can be described by a simple function:

$$t_{\rm ic} \approx 5 \times 10^{-17} T^{-2.3} E^{0.7}\ {\rm s}, \quad (42)$$

where we transformed the numerical coefficient from Equation (13) in Bosch-Ramon & Khangulyan (2009) to the units used in this paper and adopted a dilution coefficient to be 1. The comparison of Equations (40) and (42) shows that the latter implies that the function $F_{\rm iso}$ has been approximated as $F_{\rm iso} \simeq 0.4 t^{0.3}$, which provides an accuracy of <30% for $5 < t < 10^3$.

4. INTERACTION RATE

Another important characteristic of Compton scattering is the interaction rates:

$$\dot{N}_{\rm ani} = \frac{m_{\rm e}^3 c^4 \kappa}{\pi^2 \hbar^3} \int_0^\infty d\omega_0 \frac{\omega_0^2}{{\rm e}^{\omega_0/T} - 1} (1 - \cos\theta) \sigma(b_\theta), \quad (43)$$

and

$$\dot{N}_{\rm iso} = \frac{m_{\rm e}^3 c^4 \kappa}{\pi^2 \hbar^3} \int_0^\infty d\omega_0 \frac{\omega_0^2}{{\rm e}^{\omega_0/T} - 1} \times \int_{-1}^{1} \frac{d\cos\theta}{2} (1 - \cos\theta) \sigma(b_\theta), \quad (44)$$

for the scattering at a fixed interaction angle and for the angle-averaged interactions, respectively. Here, σ is the Lorentz-invariant cross section for Compton scattering (see, e.g., Berestetskii et al. 1971):

$$\sigma(x) = \frac{2\pi r_0^2}{x} \left[\left(1 - \frac{4}{x} - \frac{8}{x^2}\right) \log(1 + x) + \frac{1}{2} + \frac{8}{x} - \frac{1}{2(1+x)^2} \right]. \quad (45)$$

For the case of a fixed scattering angle, the interaction rate can be expanded as

$$\dot{N}_{\rm ani} = \frac{r_0^2 m_{\rm e}^3 c^4 \kappa}{4\pi\hbar^3 E^3 (1-cos\theta)^2} \times \int_0^\infty db_\theta \, \frac{b_\theta}{{\rm e}^{b_\theta/t_\theta}-1} \left[\left(1 - \frac{4}{b_\theta} - \frac{8}{{b_\theta}^2}\right) \log(1+b_\theta) + \frac{1}{2} + \frac{8}{b_\theta} - \frac{1}{2(1+b_\theta)^2} \right] = \frac{2 r_0^2 m_{\rm e}^3 c^4 \kappa T^2}{\pi \hbar^3 E} F_{\rm n,ani}(t_\theta) \,. \quad (46)$$

The integral term in Equation (46) has the following asymptotic behavior[7]:

$$F_{\rm n,ani}(u) = \begin{cases} \frac{4}{3}\zeta(3)\, u = 1.6\, u, & u \ll 1 \\ \frac{\pi^2}{12}\, \log(u) = 0.822 \log(u), & u \gg 1, \end{cases} \quad (47)$$

therefore in the zeroth-order approximations this function can be presented in the form:

$$G^{(0)}_{\rm n,ani}(u) = 0.822 \log(1 + 1.95u) \,. \quad (48)$$

Like in the previous cases, one can improve this approximate formula by the correction function given in Equation (20). In Figure 8, we show $G^{(0)}_{\rm n,ani}(u) \times g(u)$ for the following parameter values:

$$\alpha_{\rm n,ani} = 0.885, \quad a_{\rm n,ani} = 1.05, \quad \beta_{\rm n,ani} = 1.213, \quad b_{\rm n,ani} = 2.46 \,. \quad (49)$$

It can be seen that this approximation provides a precision at the level of 1%.

If the photon field is isotropic, the interaction rate can be expressed as

$$\dot{N}_{\rm iso} = \frac{r_0^2 m_{\rm e}^3 c^4 \kappa}{16\pi\hbar^3 E^3} \int_0^\infty \frac{db}{{\rm e}^{b/t}-1} \int_0^b dx \times \left[\left(1 - \frac{4}{x} - \frac{8}{x^2}\right) \log(1+x) + \frac{1}{2} + \frac{8}{x} - \frac{1}{2(1+x)^2} \right] = \frac{2 r_0^2 m_{\rm e}^3 c^4 \kappa T^2}{\pi \hbar^3 E} F_{\rm n,iso}(t). \quad (50)$$

Here, the integral term has properties similar to those of Equation (47):

$$F_{\rm n,iso}(u) = \begin{cases} \frac{2}{3}\zeta(3)\, u = 0.801\, u, & u \ll 1 \\ \frac{\pi^2}{12}\, \log(u) = 0.822\, u, & u \gg 1 \end{cases} . \quad (51)$$

Thus, in the zeroth-order approximation, this function can be presented as

$$G^{(0)}_{\rm n,iso}(u) = 0.822 \log(1 + 0.97u) \,. \quad (52)$$

This approximation provides relatively poor precision (at the level of <30%). However, adopting the correction function given in Equation (20), one achieves a much higher precision (better than 1%; see Figure 8) with the following set of parameters:

$$\alpha_{\rm n,iso} = 0.88, \quad a_{\rm n,iso} = 0.829, \quad \beta_{\rm n,iso} = 1.135, \quad b_{\rm n,iso} = 1.27. \quad (53)$$

Combining Equations (32), (43) and (44) one can determine the temperature dependence of the emitted photon mean energy:

$$\bar{z}_{\rm ani/iso} = \frac{1}{E} \frac{\dot{E}_{\rm ani/iso}}{\dot{N}_{\rm ani/iso}} = \frac{F_{\rm ani/iso}(u)}{F_{\rm n,ani/iso}(u)} \,. \quad (54)$$

In the case of a mono-directional photon field, the argument of the function in the above equation is $u = 2ET(1-\cos\theta)$; in the case of an isotropic photon field, the argument is $u = 4ET$.

Obviously, the approximate formulae found for the functions $F_{\rm ani}$, $F_{\rm iso}$, $F_{\rm n,ani}$, and $F_{\rm n,iso}$ (see Equations (35), (38), (39), (48), (49), (52), (53)) allow for the derivation of high-precision analytical formulae for $\bar{z}$. However, the one-parameter freedom in Equations (35) and (38) allows for a significant simplification of the expressions. Namely, in the case of a mono-directional photon field, the mean energy can be approximated as

$$\bar{z}_{\rm ani} = \frac{G^{(0)}_{\rm ani}}{G^{(0)}_{\rm n,ani}} \quad (55)$$

with $c_{\rm z,ani} \simeq 4.26$ in $G^{(0)}_{\rm ani}$ that minimizes the deviation of the approximation function from the precise expression. As seen in Figure 9, the error remains below 3%. Rounding the coefficients to one non-zero digit (i.e., keeping the precision at the level of 10%), one obtains:

$$\bar{z}_{\rm ani} = \frac{t_\theta}{t_\theta + 0.2} \frac{\log(1 + t_\theta/2)}{\log(1 + 2t_\theta)} \,. \quad (56)$$

Similarly, for the case of an isotropic photon field, the approximated formula for the fraction of the mean energy,

$$\bar{z}_{\rm iso} = \frac{G^{(0)}_{\rm iso}}{G^{(0)}_{\rm n,iso}}, \quad (57)$$

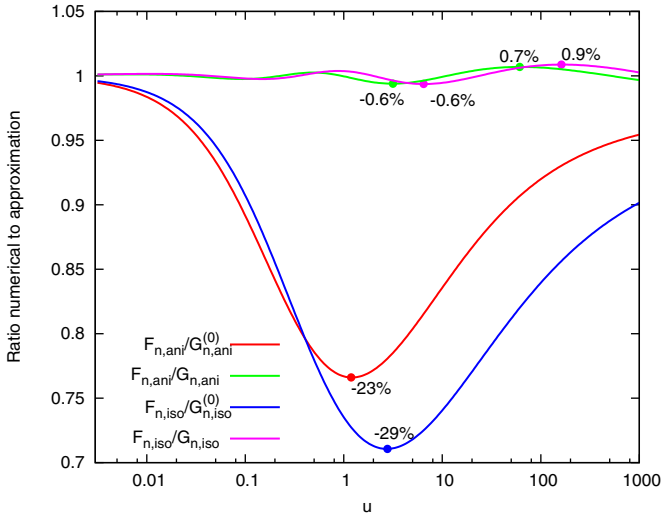

Figure 8. Ratios of the function $F_{\rm n,ani}$ to $G^{(0)}_{\rm n,ani}$ and $G^{(0)}_{\rm n,ani} \times g(u)$ and the ratios of the function $F_{\rm n,iso}$ to $G^{(0)}_{\rm n,iso}$ and $G^{(0)}_{\rm n,iso} \times g(u)$.
(A color version of this figure is available in the online journal.)

[7] Here, ζ denotes the Riemann Zeta function.

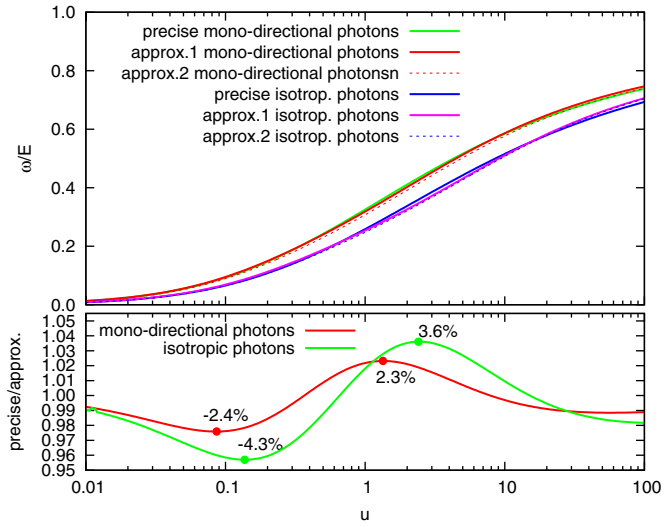

Figure 9. Upper panel: the ratio of the mean energy of the upscattered photon to the electron energy, plotted as a function of $u = t$ (for an isotropic photon field) and $u = t_\theta$ (for a mono-directional photon field). Approximation 1 corresponds to Equations (55) and (57) for the cases of mono-directional and isotropic photon fields, respectively. Approximation 2 corresponds to Equations (56) and (58) for the cases of mono-directional and isotropic photon fields, respectively. Bottom panel: ratios of numerical calculations to approximations given by Equations (55) and (57) for the cases of mono-directional and isotropic photon fields, respectively.

(A color version of this figure is available in the online journal.)

results in a 5% precision (see Figure 9) for the value of $c_{z,\rm iso} = 2.9$ in $G^{(0)}_{\rm iso}$. Rounding the coefficients to one non-zero digit, one obtains

$$\bar{z}_{\rm iso} = \frac{t}{t+0.3}\frac{\log(1+t/4)}{\log(1+t)}\,. \tag{58}$$

The mean photon energy characterizes the typical energy band of upscattered photons in which an electron loses its energy via the IC process. Note that in many cases the inverse problem is more common, i.e., a reconstruction of the electron energy on the basis of the observed photon energy and the temperature of the target photons. In other words, one needs to solve the transcendental Equation (58) (or Equation (56)), to obtain t (or, respectively, t_θ) as a function of $\bar{\omega}$ and T. Using Equations (56) and (58), one can derive the following approximate solution:

$$t_{\theta/.} = \frac{v^{1/2}(1+2v^{1/2})}{2}\sqrt{\frac{\log(1+v^{1/2})}{\log(1+v^{1/2}/V_0)}}, \tag{59}$$

which allows one to obtain the lepton energy with $<10\%$ precision over the entire range of parameters. One should adopt $V_0 = 3$ and $v = 2\bar{\omega}T(1-\cos\theta)$ for the case of a mono-directional photon field and $V_0 = 4$ and $v = 4\bar{\omega}T$ for an isotropic distribution of photons.

5. IMPACT OF RELATIVISTIC MOTION

The formulae presented in the previous sections correspond to the reference system, where the source of photons is at rest (we refer to this system as K). Since the particle distribution can be always transformed to this coordinate system, these formulae can, in principle, cover all the required calculations. However, under certain conditions it is more convenient to perform calculations in another coordinate system, K' (the physical quantities measured in this system are marked with prime, i.e., ω'_0). In the case that the target photons are mono-directional in the reference frame K (in the relevant region of space), the transformation of the obtained formulae is straightforward. Indeed, in this case, the photon distribution function in the six-dimensional momentum-coordinate phase space ($dN = \rho\, d^3\mathbf{p}d^3\mathbf{r}$) has the following form:

$$\rho(\mathbf{p},\mathbf{r}) = \delta(\mathbf{n_p}-\mathbf{n}_0)\frac{c}{p^2}n_{\rm ph}(\omega_0), \tag{60}$$

where $\mathbf{n_p} = \mathbf{p}/p$, $\omega_0 = cp$, and $\mathbf{n}_0$ is the unit vector corresponding to the direction of photons in the system K. Function $n_{\rm ph}$ corresponds to the energy distribution of the target photons, i.e., $dN_{\rm ph} = n_{\rm ph}d\omega_0$, and in the system K is Planckian. The function ρ is a Lorentz invariant (see, e.g., Landau & Lifshitz 1975), i.e., $\rho(\mathbf{p},\mathbf{r}) = \rho'(\mathbf{p}',\mathbf{r}')$, and it can be shown that, in this specific case, the function $n_{\rm ph}$ is an invariant as well:

$$n'_{\rm ph}(\omega'_0) = n_{\rm ph}(\omega_0)\,. \tag{61}$$

Here, target photon energies ω_0 and ω'_0 are related via the Lorentz transformation: $\omega_0 = \mathcal{D}_*\omega'_0$, where $\mathcal{D}_* = [\Gamma(1-(v_0/c)\cos\chi)]^{-1}$ is the Doppler factor between the source of blackbody photons (reference system K) and the gamma-ray production region (reference system K') moving with relative velocity v_0, which makes an angle χ to the photon momentum (the variable $\Gamma = (1-(v_0/c)^2)^{-1/2}$ denotes the bulk Lorentz factor). Since the function $n_{\rm ph}(\omega_0)$ in Equation (61) is determined by Equation (4), one can see that in the moving coordinate system K' the Planckian distribution of photons is preserved, but the temperature of the photon field is corrected for the bulk motion:

$$T' = D_*^{-1}T\,, \tag{62}$$

and an additional dilution factor is applied:

$$\kappa' = \mathcal{D}_*^2\,. \tag{63}$$

Equations (62) and (63) allow for a generalization of the formulae obtained in the previous sections for the case of a mono-directional photon field to a moving system K'. As it follows from their derivations, Equations (60) and (61) do not account for the relativistic effects related to the transformation of the IC emission from the source frame to the observer frame (for details, see, e.g., Rybicki & Lightman 1979; Jester 2008). Also, we note that the interaction angle, θ, should be transformed to the system K'. The transformation of the interaction angle can be readily obtained by considering the scalar product of the four-momenta of the electron and the target photon (i.e., a Lorentz invariant quantity). Finally, in the case when the emitting particles are isotropized in the reference frame K', the energy loss rate is described by Equation (36) with corrections imposed by Equations (62) and (63).

We leave as beyond the scope of this paper the transformation of a photon field isotropic in the system K to the moving system K'. If looked at from the system K', such a photon field is not an isotropic field, therefore the basic equation (Equation (3)) is not applicable for the description of the IC scattering process. If the bulk Lorentz factor is large, $\Gamma \gg 1$, the photon field in the K' system appears to be nearly mono-directional, with photons moving against the bulk velocity. However, the energy distribution of the photons in this case deviates significantly from the Planckian distribution. We note, however, that in the case of an isotropic photon field, the distribution of electrons can be transformed to the system K and the formulae obtained for the spectrum can be used.

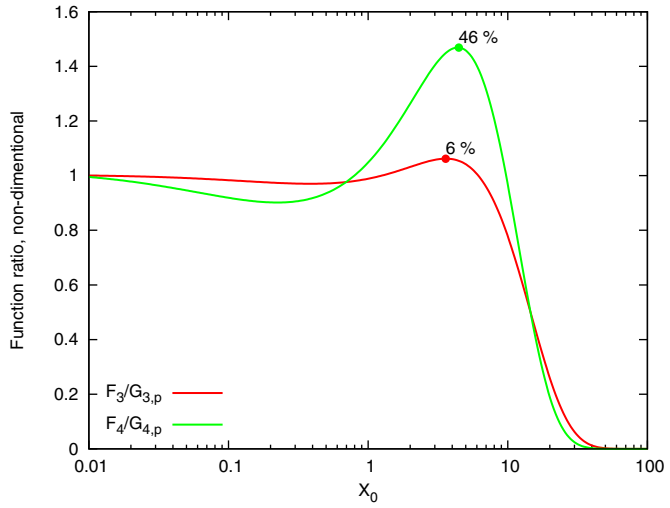

Figure 10. Comparison of the approximation proposed by Petruk (2009) with the numerical calculations.

(A color version of this figure is available in the online journal.)

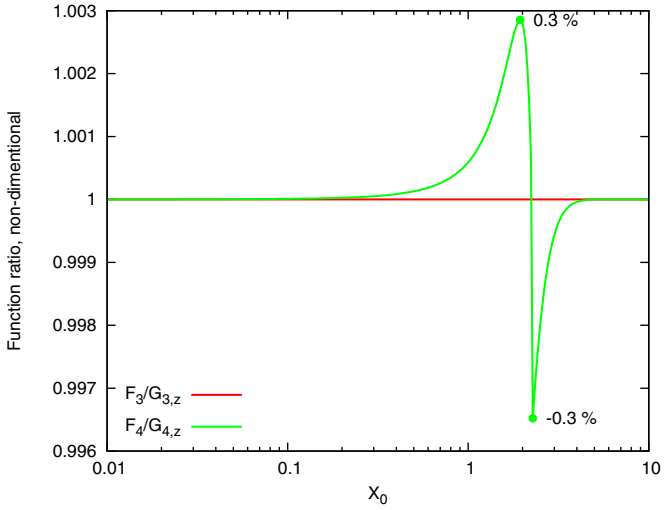

Figure 11. Comparison of the approximation proposed by Zdziarski & Pjanka (2013) with the numerical calculations.

(A color version of this figure is available in the online journal.)

6. COMPARISON WITH OTHER APPROACHES

In order to simplify calculations, one may try to replace the relatively narrow Planckian distribution by the δ function, or alternatively, use a simplified description of the cross section, e.g., the Heaviside step function (Petruk 2009). For the sake of brevity, in what follows, we discuss the δ-functional approximation for a mono-directional target photon field and the step function approximation of Petruk (2009) for the scattering off an isotropic photon field.

The δ-functional approximation for target photons assumes the following photon field:

$$\frac{dN_{\rm ph}}{d\omega_0} \simeq n_*\delta(\omega_0-\omega_*)\,. \tag{64}$$

It is easy to be convinced that for $n_* = (2\zeta(3)m_{\rm e}^3c^3\kappa T^3)/(\pi^2\hbar^3)$ and $\omega_* = \pi^4/(30\zeta(3))\,T \simeq 2.7\,T$ one can reproduce correctly both the number and energy densities of the Planckian photon field. However, to a certain extent, the choice of these parameters is arbitrary.

The substitution of Equation (64) into Equation (7) results in the following expression:

$$\frac{dN_{\rm ani}}{d\omega\,dt} = \frac{2r_o^2m_{\rm e}^3c^4\kappa T^2}{\pi\hbar^3E^2}\left[\frac{z^2}{2(1-z)}G_{1,\delta}(x_0)+G_{2,\delta}(x_0)\right], \tag{65}$$

where

$$G_{1,\delta}(x_0) = \frac{n_*\hbar^3\pi^2}{\kappa T^2\omega_* m_{\rm e}^3c^3}\Theta\left(\frac{\omega_*}{T}-x_0\right) \tag{66}$$

and

$$G_{2,\delta}(x_0) = \frac{n_*\hbar^3\pi^2}{\kappa T^2\omega_* m_{\rm e}^3c^3}\Theta\left(\frac{\omega_*}{T}-x_0\right) \times\left(1-\frac{2x_0}{\omega_*/T}+\frac{2x_0^2}{(\omega_*/T)^2}\right). \tag{67}$$

Here, $\Theta(x_0)$ is the Heaviside step function.

The comparison of Equations (66) and (12) and Equations (67) and (13) allows us to estimate the errors introduced by the δ-functional approximation: (1) the lower energy part of the spectrum ($x_0 \ll 1$) can be reproduced quite well if the selected parameters satisfy the condition $n_*/(T^2\omega_*) = \kappa m_{\rm e}^3c^3/(6\hbar^3)$ and (2) the accuracy declines significantly for the high-energy part ($x_0 \gtrsim 1$). The δ function imposes an artificial cutoff at $x_0 = \omega_*/T$. Also, the accuracy close to the cutoff appears to be quite poor. For example, the accuracy of the term $G_{1,\delta}$ can be estimated as $G_{1,\delta}/G_1^{(0)}$, which gives a factor of three error for $x_0 = 2$ (assuming that $\omega_*/T > 2$, as commonly adopted).

Similarly, it can be shown that for the cross section averaged over the interaction angle, the δ-functional approximation gives a similar precision. This means that although a practical realization of the δ-functional approximation is characterized by a similar complexity as the approach suggested in this paper, the accuracy provided by the δ-functional approximation is very poor, especially in the Klein–Nishina regime.

A more complicated approach has been suggested by Petruk (2009) for the case of the cross section averaged over the interaction angle. In this approach, the IC cross section was approximated by a step function and integrated over the Planckian photon distribution. This approximation can be expressed as

$$\frac{dN_{\rm iso}}{d\omega\,dt} = \frac{2r_o^2m_{\rm e}^3c^4\kappa T^2}{\pi\hbar^3E^2}\left[\frac{z^2}{2(1-z)}G_{3,\rm p}(x_0)+G_{4,\rm p}(x_0)\right], \tag{68}$$

where

$$G_{3,\rm p}(x_0) = \frac{\pi^2}{6}{\rm e}^{-\frac{2}{3}x_0-\frac{5}{7}x_0^{0.7}} \tag{69}$$

and

$$G_{4,\rm p}(x_0) = \frac{\pi^2}{6}{\rm e}^{-\frac{2}{3}x_0-\frac{5}{4}x_0^{0.5}}\,. \tag{70}$$

In Figure 10, we compare the approximation of Petruk (2009) with precise numerical calculations and arrive at a conclusion, similar to the statement of Zdziarski & Pjanka (2013), that for certain parameters this approximation cannot guarantee a precision better than ~50% (we note that Petruk 2009, did not approximate the cross section in the region of the exponential tail, i.e., for $x_0 \gg 1$).

Finally, Zdziarski & Pjanka (2013) suggested an analytical method to describe Equations (2) and (3) based on the truncation of series, which describe the functions f_{-1} and $f_{\rm ln}$. In Figure 11,

Table 1
Derived Parameterizations

Function	Used in Equations	Approximated Description		Fit Parameters Values					Precision	Figure
		Function	Variable	a	α	b	β	c		
			Representation of spectra							
F_1	Equation (11)	$G_1^{(0)} = \left(\frac{\pi^2}{6} + x_0\right) e^{-x_0}$	$\frac{z}{1-z}\frac{1}{2ET(1-\cos\theta)}$	...	...	...	...	...	~10%	Figures 1 and 2
F_1	Equation (11)	$G_1^{(0)}(x_0) \times g(x_0)$	$\frac{z}{1-z}\frac{1}{2ET(1-\cos\theta)}$	0.153	0.857	0.254	1.84	...	<1%	Figures 1 and 2
F_2	Equation (11)	$G_2^{(0)} = \left(\frac{\pi^2}{6} + x_0\right) e^{-x_0}$	$\frac{z}{1-z}\frac{1}{2ET(1-\cos\theta)}$	...	...	...	...	...	~50%	Figures 1 and 3
F_2	Equation (11)	$G_2^{(0)}(x_0) \times g(x_0)$	$\frac{z}{1-z}\frac{1}{2ET(1-\cos\theta)}$	1.33	0.691	0.534	1.668	...	<1%	Figures 1 and 3
F_3	Equation (14)	$G_3^{(0)} = \frac{\pi^2}{6}\frac{1+c\,x_0}{1+\frac{\pi^2 c}{6}x_0} e^{-x_0}$	$\frac{z}{1-z}\frac{1}{4ET}$	...	...	...	...	2.73	~3%	Figures 4 and 5
F_3	Equation (14)	$G_3^{(0)}(x_0) \times g(x_0)$	$\frac{z}{1-z}\frac{1}{4ET}$	0.443	0.606	0.54	1.481	0.319	<1%	Figures 4 and 5
F_4	Equation (14)	$G_4^{(0)} = \frac{\pi^2}{6}\frac{1+c\,x_0}{1+\frac{\pi^2 c}{6}x_0} e^{-x_0}$	$\frac{z}{1-z}\frac{1}{4ET}$	...	...	...	...	47.1	~30%	Figures 4 and 6
F_4	Equation (14)	$G_4^{(0)}(x_0) \times g(x_0)$	$\frac{z}{1-z}\frac{1}{4ET}$	0.726	0.461	0.382	1.457	6.62	<1%	Figures 4 and 6
			Energy losses							
$F_{\rm ani}$	Equations (33) and (55)	$G_{\rm ani}^{(0)} = \frac{cu\log(1+2.16u/c)}{1+cu/0.822}$	$2ET(1-\cos\theta)$	...	...	...	—	6.13	~1%	Figure 7
$F_{\rm iso}$	Equations (36) and (57)	$G_{\rm iso}^{(0)} = \frac{cu\log(1+0.722u/c)}{1+cu/0.822}$	$4ET$	...	...	...	—	4.62	~5%	Figure 7
$F_{\rm iso}$	Equation (36)	$G_{\rm iso}^{(0)}(u) \times g(u)$	$4ET$	−0.362	0.682	0.826	1.281	5.68	~1%	Figure 7
			Interaction rate							
$F_{\rm n,ani}$	Equations (46) and (55)	$G_{\rm n,ani}^{(0)} = 0.822\log(1+1.949u)$	$2ET(1-\cos\theta)$	...	...	...	...	...	~25%	Figure 8
$F_{\rm n,ani}$	Equation (46)	$G_{\rm n,ani}^{(0)}(u) \times g(u)$	$2ET(1-\cos\theta)$	1.05	0.885	2.46	1.213	...	~1%	Figure 8
$F_{\rm n,iso}$	Equations (50) and (57)	$G_{\rm n,iso}^{(0)} = 0.822\log(1+0.97u)$	$4ET$	...	...	...	...	...	~30%	Figure 8
$F_{\rm n,iso}$	Equation (50)	$G_{\rm n,iso}^{(0)}(u) \times g(u)$	$4ET$	0.829	0.88	1.27	1.135	...	~1%	Figure 8
			Mean energy of emitted photons							
$\bar{z}_{\rm ani}$	Equation (55)	$G_{\rm ani}^{(0)}/G_{\rm n,ani}^{(0)}$	$2ET(1-\cos\theta)$	...	...	...	—	4.26	~3%	Figure 9
$\bar{z}_{\rm ani}$	Equation (56)	$\frac{u}{u+0.2}\frac{\log(1+u/2)}{\log(1+2u)}$	$2ET(1-\cos\theta)$	...	...	...	—	...	~8%	Figure 9
$\bar{z}_{\rm iso}$	Equation (57)	$G_{\rm iso}^{(0)}/G_{\rm n,iso}^{(0)}$	$4ET$	...	...	...	—	2.9	~5%	Figure 9
$\bar{z}_{\rm iso}$	Equation (58)	$\frac{u}{u+0.3}\frac{\log(1+u/4)}{\log(1+u)}$	$4ET$	...	...	...	—	...	~8%	Figure 9
			Energy of emitting particle							
t_θ	Equation (59)	$\frac{v^{1/2}(1+2v^{1/2})}{2}\sqrt{\frac{\log(1+v^{1/2})}{\log(1+v^{1/2}/3)}}$	$2\bar{\omega}T(1-\cos\theta)$	...	...	...	—	...	~10%	...
t	Equation (59)	$\frac{v^{1/2}\left(1+2v^{1/2}\right)}{2}\sqrt{\frac{\log(1+v^{1/2})}{\log(1+v^{1/2}/4)}}$	$4\bar{\omega}T$	...	...	...	—	...	~10%	...

Notes. A typical parameterization consists of a zeroth-order approximation function, $G_{...}^{(0)}$, multiplied by the correction factor g. The zeroth-order approximation depends on the variable, which is listed in the fourth column of the table, and, in some cases, on the parameter c. The correction factor is given by Equation 20 and depends on the same variable as the zeroth-order approximation and four parameters (a, α, b, and β).

we compare precise numerical calculations for the approximated values, $G_{3,z}$ and $G_{4,z}$, that were obtained by substitution of Equations (7), (8), (14), and (28) from Zdziarski & Pjanka (2013) (the value of $N = 3$, as suggested by the authors, was adopted) into Equations (15) and (16). Since Zdziarski & Pjanka (2013) obtained analytical expressions for the functions f_{+1} and f_0, the function $G_{3,z}$ is strictly equal to F_3, which can be seen in Figure 11. The accuracy provided by the function $G_{4,z}$ is very high, at the level of 0.3%[8] (see Figure 11).

The approach by Zdziarski & Pjanka (2013) can provide an arbitrary precision (simply by increasing the number of preserved terms in the series), however, in our view, it also contains a certain shortcoming. Namely, this approach implies the usage of special functions (dilogarithm and exponential integral), which may limit practical usage.

Another important difference of our approach is that while in other studies one provides an approximate description for the cross section, we suggest an approach for a common description of all the relevant processes of IC scattering on the blackbody photons: scattering rates, energy losses, cross sections, and mean photon energy. Also, all of the approximations use the same type of correction function, Equation (20).

7. SUMMARY

In this paper, we suggest simple analytical presentations for calculations of different characteristics (differential spectra, interaction rates, and energy losses) of the IC scattering of relativistic electrons in a radiation field that is described by the Planckian distribution. Two different types of angular distribu-

[8] This accuracy is worse by approximately a factor of 10 than the accuracy of $<2.4\times10^{-4}$ achieved for the functions f_{-1} and $f_{\ln}$ (Zdziarski & Pjanka 2013). This discrepancy is explained by the fact that these functions enter into the expression for the cross section with different signs and the subtraction of these functions results in an overall error significantly exceeding the accuracy of the individual terms.

tion of the target radiation field, namely, mono-directional and isotropic distributions, have been considered.

The obtained parameterizations are characterized by a high precision, of the order of 1%, and cover the entire parameter space, allowing for an accurate description of the IC scattering in the Thomson and Klein–Nishina limits, as well as in the transition region. The derived formulae preserve the precise asymptotic behavior and have similar structures, which simplifies their practical usage (see Table 1).

The main objective of the obtained approximate analytical presentations is the fast, but convenient and accurate, calculations of characteristics of the upscattered IC emission in radiation fields described by a Planckian distribution. At the same time, the simple forms of these parameterizations allow for the derivation of some useful relations. In particular, we propose simple formulae which, for the given temperature of target photons, relate the mean energy of the electrons and upscattered photons.

REFERENCES

Aharonian, F., Akhperjanian, A. G., Bazer-Bachi, A. R., et al. 2006, A&A, 460, 743
Aharonian, F. A., & Atoyan, A. M. 1981, Ap&SS, 79, 321
Berestetskii, V. B., Lifshitz, E. M., & Pitaevskii, L. P. 1971, Relativistic Quantum Theory (Oxford: Pergamon)
Blumenthal, G. R., & Gould, R. J. 1970, RvMP, 42, 237
Bosch-Ramon, V., & Khangulyan, D. 2009, IJMPD, 18, 347
Jester, S. 2008, MNRAS, 389, 1507
Jones, F. C. 1968, PhRv, 167, 1159
Khangulyan, D., Aharonian, F. A., Bogovalov, S. V., & Ribó, M. 2011, ApJ, 742, 98
Khangulyan, D., Hnatic, S., Aharonian, F., & Bogovalov, S. 2007, MNRAS, 380, 320
Landau, L. D., & Lifshitz, E. M. 1975, The Classical Theory of Fields (Oxford: Pergamon)
Petruk, O. 2009, A&A, 499, 643
Rybicki, G. B., & Lightman, A. P. 1979, Radiative Processes in Asrtophysics (New York: Wiley)
Zdziarski, A. A., & Pjanka, P. 2013, MNRAS, 436, 2950